ZnO as a Tunable Metal: New Types of Surface Plasmon Polaritons

S. Kalusniak, S. Sadofev, and F. Henneberger
Institut für Physik, Humboldt Universität zu Berlin, Newtonstraße 15, 12489 Berlin, Germany
(Received 12 September 2013; published 1 April 2014)

The use of the free-electron gas in a heavily doped semiconductor (ZnO:Ga) enables the realization of almost arbitrarily shaped surface-plasmon-polariton dispersion curves in planar geometries. In particular, by preparing metal-metal-type interfaces, we demonstrate surface-plasmon polaritons exhibiting finite frequencies in the long-wavelength limit. Moreover, coupling of surface plasmon polaritons at adjacent interfaces allows for the controlled formation of frequency gaps or, alternatively, the opening of otherwise forbidden regions by an appropriate layer design. Our findings reveal a considerable plasmonic potential of this semiconductor-based approach, e.g., for achieving propagation control or phase matching for nonlinear optical processes as well as novel many-particle phenomena.

DOI: 10.1103/PhysRevLett.112.137401 PACS numbers: 78.66.-w, 42.25.-p, 73.20.Mf, 78.67.Pt

The interaction of metals with electromagnetic radiation gives rise to collective charge excitations called surface plasmon polaritons (SPPs) [1]. The potential of these coupled light-matter states for creating nanoscale photon-based circuits is the core of what is summarized today by the term "plasmonics" [2]. Seminal examples involving SPPs are the subwavelength control of light [3,4], below-diffraction-limit microscopy [5], or biosensing [6], to name only a few. However, currently available plasmonic functions are still constrained by the limited ability to tailor the SPP's frequency versus wave vector dispersion, even when utilizing modern nanofabrication techniques. Here, we show that use of the free-electron gas in a heavily doped semiconductor enables the realization of almost arbitrarily shaped SPP dispersion curves, not only by tuning of the dielectric function but also by coupling of SPPs in planar multilayer structures. In particular, by preparing metal-metal-type interfaces, we demonstrate SPPs exhibiting finite frequencies in the long-wavelength limit, in marked contrast to the conventional dielectric-metal SPPs. Moreover, the controlled formation of frequency gaps or, alternatively, the opening of otherwise forbidden regions is accomplished by an appropriate layer design.

Recently, semiconductors where heavy doping can produce a metallic dielectric function have been identified as promising plasmonic materials for the infrared spectral range [7,8]. In particular, ZnO normally fully infrared transparent outside the reststrahlen band has turned out to be a suitable candidate with low plasmonic loss, even up to telecommunication wavelengths [9–11]. In this Letter, we go one essential step further by utilizing the semiconductor-specific ability to tune the free-electron concentration and to fabricate low-roughness interfaces separating two different "metals". The dispersion relation of SPPs at such an interface was outlined many years ago [12]. However, for conventional metals, the relevant frequencies are outside the optical range and cannot be easily accessed. Previous related work is, thus, restricted to the analysis of ultrathin-film deposition of metals on metals [13], space charge layers in semiconductors junctions [14], or dielectric transition layers with strong resonances on metals [15]. None of these studies has addressed or demonstrated the distinctive metal-metal dispersion features, nor have there been efforts to exploit them in a plasmonic context.

The Ga-doped ZnO layers used in this study are grown by molecular beam epitaxy on *a*-plane sapphire [11]. The films are characterized by *in situ* reflection high-energy electron diffraction and post-growth high-resolution x-ray diffraction to monitor structural quality. Control of doping level and free-electron concentration within a few percent is achieved by secondary ion mass spectroscopy in combination with Hall measurements. Angle-dependent reflectivity and transmission as well as attenuated total reflection (ATR) spectra are recorded by a Bruker IFS66v/s vacuum Fourier transform spectrometer. The angle of incidence is controlled by a motorized A-513 reflection unit with an accuracy of better than 2°. ATR measurements are performed in Otto configuration using a polished silicon hemisphere as coupling medium. The samples are mounted on a high-pressure spring to achieve intimate contact between sample surface and basis of the hemisphere. The remaining air gap formed by this procedure is typically 200–500 nm thick, as derived from the interference fringes observed from the specimen's sapphire backside under white-light illumination. Absolute values of the reflectivity are obtained by measuring reference spectra of the sole silicon hemisphere.

As a first step, we present SPP dispersions deduced from ATR measurements on single ZnO films at different doping levels. While the ATR spectra are featureless in transverse electric (TE) polarization (see the Supplemental Material [16]), a pronounced minimum occurs in transverse magnetic (TM) geometry [Fig. 1(a)]. As shown in Fig. 1(b), the experimental spectra are very well reproduced by transfer

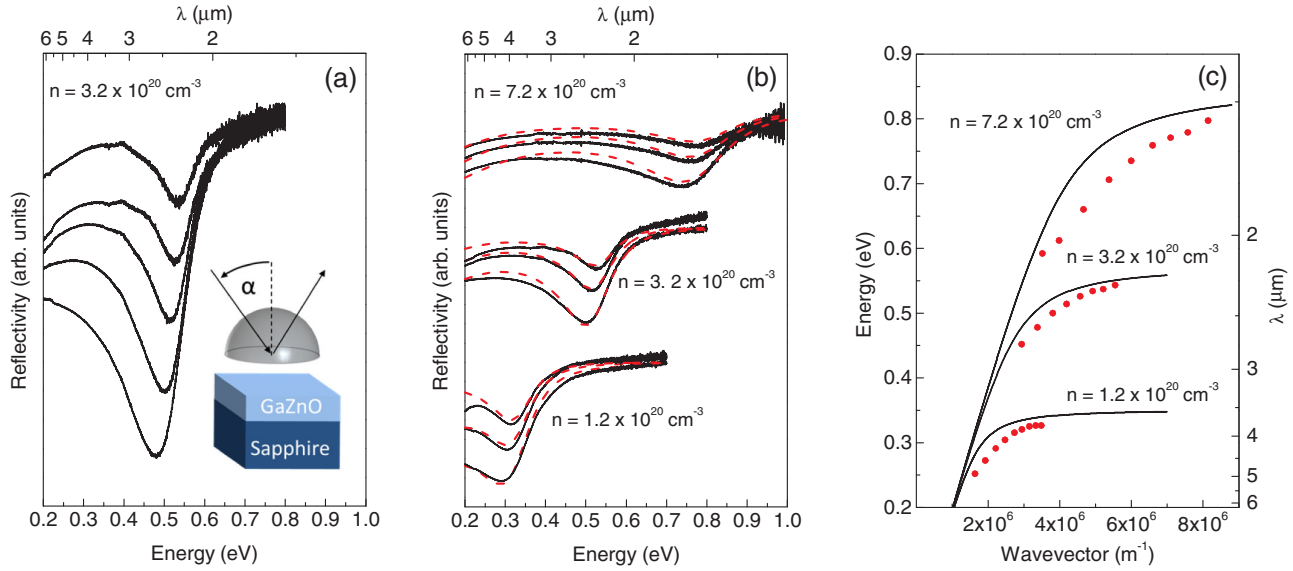

FIG. 1 (color online). SPPs at a single GaZnO/air interface. (a) ATR spectra (TM polarization) of a layer with a free-electron concentration $n = 3.2 \times 10^{20}$ cm^{-3} at various angles of incidence $\alpha = 32°, 30°, 28°, 26°, 24°$. The inset schematizes the ATR configuration where a silicon hemisphere is used to excite evanescent waves along the surface plane. (b) ATR spectra of three samples with different free-electron concentrations at three selected angles of incidence (upper set: $\alpha = 32°, 30°, 28°$, two lower sets: $\alpha = 30°, 28°, 26°$). Continuous black curves: experiment. Red dashed curves: TRMA calculations ($\gamma = 224$, 120, and 118 meV, air gap = 250, 415, and 495 nm). (c) Dispersion relations deduced for the free-electron concentrations of (b). Circles: experimental ATR minima. Curves: calculated from Eq. (2) with predetermined dielectric-function parameters (see text). All denoted parameters change from top to bottom. The thickness of the GaZnO layers is always 400 nm.

matrix (TRMA) calculations for the ATR setting [inset of Fig. 1(a)] accounting for the silicon hemisphere as a semi-infinite medium ($\epsilon_{\mathrm{Si}} = 11.8$), the air gap ($\epsilon_{\mathrm{air}} = 1$), the GaZnO layer described by Drude's dielectric function

$$\epsilon(\omega) = \epsilon_B - \frac{\omega_p^2}{\omega(\omega + i\gamma)} \tag{1}$$

as well as the (semi-infinite) sapphire substrate ($\epsilon = 2.89$). In Eq. (1), $\epsilon_B = 3.7$ is the background dielectric constant, $\omega_p = (e^2 n/\epsilon_0 m_e)^{1/2}$ the plasma frequency, $m_e = 0.29 m_0$ the effective mass of the electrons, and γ the scattering rate. Applicability of this dielectric function in the relevant spectral range has been validated previously by standard reflection and transmission measurements on a large set of GaZnO samples [11]. Especially, the n-dependent scattering rates were deduced from these spectra and additionally verified by Hall-mobility measurements. All calculations presented in this work are, thus, carried out with reliable, predetermined dielectric-functions parameters. Figure 1(c) represents plots of the ATR minima versus the in-plane wave vector $k = \omega/c\sqrt{\epsilon_{\mathrm{Si}}}\sin\alpha$ realized for the respective angle of incidence α. The data points are located clearly right of the photon line ($\omega = ck$) and correlate well with the theoretically expected dispersion relation calculated for the air/GaZnO interface from (see, e.g., Ref. [15]),

$$[1 + \epsilon(\omega)]c^2k^2 = \omega^2\epsilon(\omega). \tag{2}$$

Note that the exact position of the ATR minima depends on the thickness of the air gap, which is the least accurately known quantity in our study and that is fine adjusted such that experimental and calculated ATR minima best match (see the Supplemental Material [16]). Figure 1 directly demonstrates that the spectral location of the GaZnO/air SPP modes can be tuned via the doping level from the midinfrared up to the telecommunication wavelength of 1.55 μm.

Interfaces between differently doped GaZnO layers are not only suited to produce the targeted metal-metal SPP dispersion. In addition, when properly embedded in multilayer structures, novel interaction geometries of SPPs are formed, providing immense flexibility to construct almost arbitrarily shaped dispersion curves for a desired plasmonic function. In what follows, we represent two paradigmatic examples documenting this potential. The design of the structures schematized in Fig. 2(a) consists of a thicker GaZnO substrate film No. 2 (400 nm) on top of sapphire followed by a thinner GaZnO layer No. 1 of width $d =$ 100 nm constituting the interface to air. For reasons that become clear below, the doping level is adjusted such that $\omega_{\mathrm{p1}} > \omega_{\mathrm{p2}}$ holds for both samples. Whereas the difference between the plasma frequencies is quite small for sample A ($\omega_{\mathrm{p1}}^2 \approx 2\omega_{\mathrm{p2}}^2$), $\omega_{\mathrm{p1}}^2 \approx 10\omega_{\mathrm{p2}}^2$ is realized for sample B. Solving the coupled system of Schrödinger and Poisson equation yields a transition width of about 10 nm for the free-electron concentration at the present doping levels so

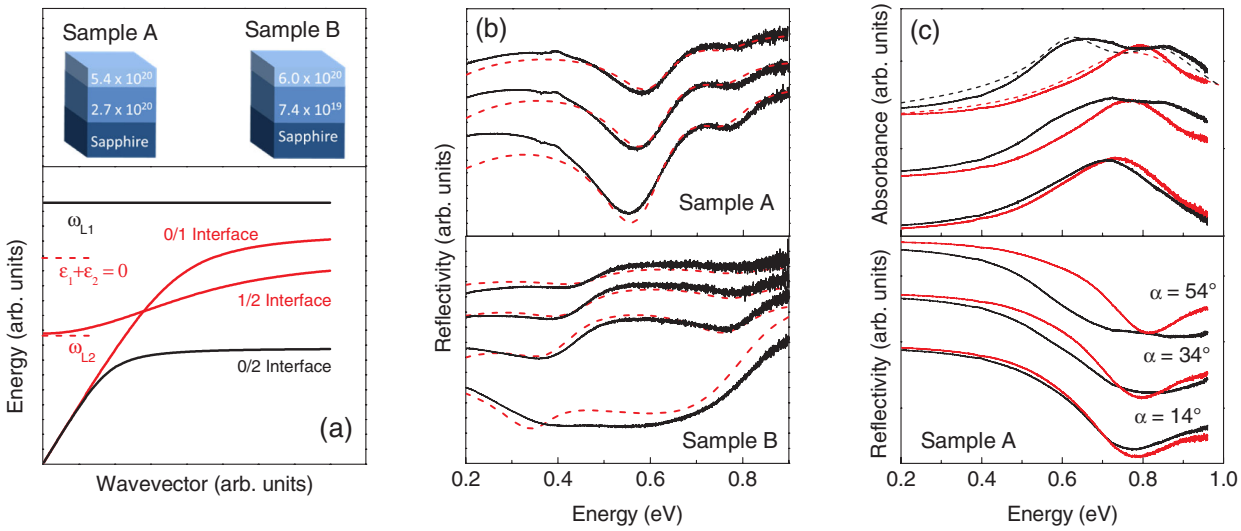

FIG. 2 (color online). SPPs at a GaZnO/GaZnO/air double interface. (a) Top: sample design. Numbers are the free-electron densities in cm^{-3}. Bottom: schematic plot of the SPP dispersion curves for interface separation $d \to 0$ (black line) and $d \to \infty$ (red lines) for lossless materials ($\gamma = 0$). (b) ATR spectra (TM polarization) of sample A (upper panel, $\alpha = 30°, 28°, 26°$) and sample B (lower panel, $\alpha = 38°, 34°, 30°, 22°$). Continuous black curves: experiment. Red dashed curves: TRMA calculations (A: $\gamma_1 = 136$ meV, $\gamma_2 = 112$ meV, B: $\gamma_1 = 164$ meV, $\gamma_2 = 90$ meV). (c) Free-space reflection (lower panel) and absorption spectra (upper panel) of sample A for the same α set. Full curves: TE (red) and TM (black) polarization. Exemplary, a TRMA calculation for $\alpha = 54°$ is added (dashed curves).

that these profiles can be approximated by step functions in this study.

The ATR spectra of the air/GaZnO/GaZnO/sapphire structures exhibit two minima clearly proving the existence of two different types of SPPs [Fig. 2(b)]. Again, the experimental spectra agree very well with TRMA calculations for the two-interface setting. The dispersion relations in the presence of two planar interfaces separated by a distance d follow from [15,16]

$$(\beta_0 + \beta_1)(\beta_1 + \beta_2) + (\beta_0 - \beta_1)(\beta_1 - \beta_2)e^{-2q_1 d} = 0, \quad (3)$$

with the admittances $\beta_j(\omega, k) = \epsilon_j(\omega)/q_j(\omega, k)$, $j = 0, 1, 2$, $\epsilon_0 = \epsilon_{\text{air}} = 1$, and $q_j(\omega, k) = \sqrt{k^2 - (\omega/c)^2 \epsilon_j(\omega)}$ where iq_j represents the wave vector component normal to the interfaces. In the limit $d \to 0$, this equation simplifies to $\beta_1(\beta_0 + \beta_2) = 0$ providing as solutions the longitudinal plasma frequency $\epsilon_1(\omega_{L1}) = 0$ of the electron gas of layer No. 1 as well as the air/GaZnO♯2 dispersion $\beta_0 = -\beta_2$. On the other hand, for $d \to \infty$, it results in $\beta_0 = -\beta_1$ and $\beta_1 = -\beta_2$, i.e., the SPP dispersions of the uncoupled interfaces air/GaZnO♯1 and GaZnO♯1/GaZnO♯2, respectively. $\beta_1 = -\beta_2$ can be recast into

$$[\epsilon_1(\omega) + \epsilon_2(\omega)]c^2k^2 = \omega^2 \epsilon_1(\omega)\epsilon_2(\omega) \quad (4)$$

i.e., the isolated metal-metal ω-k-relation is confined to the range where $\epsilon_1 + \epsilon_2 < 0$ but with a negative dielectric function of only one of the metals. As already stressed above, it starts on the long-wavelength side ($k \to 0$) at finite frequency, $\omega_{L2} = \omega_{p2}/\sqrt{\epsilon_B}$ for the present samples, and approaches $\omega_{12}^{\infty} = \sqrt{(\omega_{p1}^2 + \omega_{p2}^2)/\epsilon_B}$ at large in-plane wave vector. From the plot of the two limiting cases in Fig. 2(a), it is obvious that the dispersion relations undergo profound changes as a function of d and that the interface separation is, thus, a key parameter for engineering their shape (Supplemental Material [16]). The 100-nm thickness of the upper GaZnO♯1 layer in our samples is chosen such that it is—on the one hand—thin enough to allow for simultaneous excitation of both interfaces by the incident light and—on the other hand—large enough to ensure the formation of a metal-metal-type dispersion relation.

Figure 3(a) depicts the observed ATR minima together with numerically calculated dispersion curves ($\text{Re}\,\omega$) for sample A. Consistent with the evaluation of spectra at given angle of incidence, Eq. (3) is solved for complex ω at real k. While the dispersion curves of the isolated SPPs ($d \to \infty$) plotted for reference cross and are almost degenerate beyond the intersection, the corresponding branches 1 and 2 of the double interface stay clearly separated. For large k values, the frequency of branch 2 markedly exceeds ω_{12}^{∞} and even draws near ω_{L1}. These findings directly evidence significant interaction of the SPPs in this wave vector region. On the long-wavelength side, branch 2 closely follows that of the isolated metal-metal interface and ends up, indeed, at finite frequency. In addition, a further branch 3 is present as a leftover of the flat ω_{L1} dispersion at $d = 0$. It stops close to the photon line. SPP states left of the photon line cannot be accessed in the ATR setup and have been uncovered as described below.

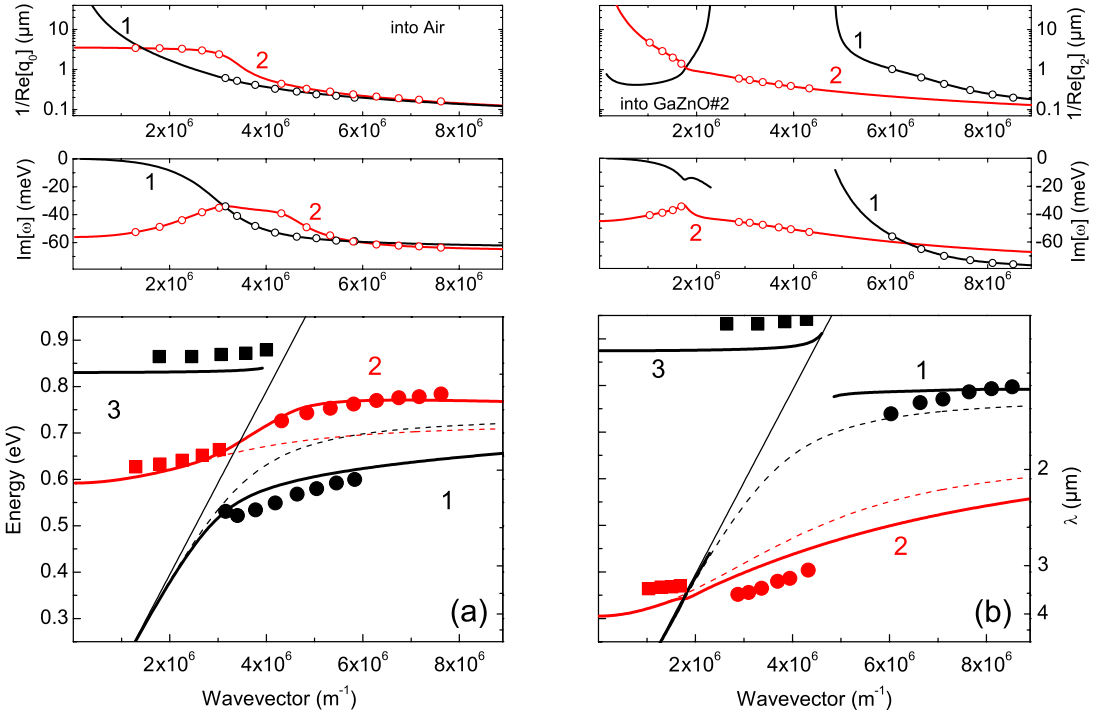

FIG. 3 (color online). Dispersion relations of coupled SPPs. (a) Sample A. (b) Sample B. Circles: experimental ATR minima. Rectangles: derived from the experimental free-space absorption maxima (Supplemental Material [16]). Dashed curves: calculated dispersion for the isolated $0/1$ (black) and $1/2$ (red) interface. Full curves: dispersion relation (Re ω) deduced for the coupled SPP states. Thin line: $\omega = ck$. Upper panels: calculated damping rates (Im ω) and examples of calculated penetrations depths. To guide the eye, open circles were set on the curves at the positions where the existence of the respective SPP is experimentally confirmed.

The character of the SPPs becomes evident from their damping rates (Im ω) as well as from the penetration depths in the media determined by the inverse imaginary part of the normal wave vector components ($1/\mathrm{Re}\, q_j$). Examples are displayed in the upper panels of Fig. 3. While the damping rate of the standard-type lower dispersion 1 declines when approaching the photon line, Im ω stays always close to the scattering rates of the free-electron gases for branch 2, signifying a predominant plasmonic nature of these metal-metal SPPs. Furthermore, their field penetration into air remains finite for $k \to 0$ so that surface localization on the wavelength scale is always maintained.

For sample B with a larger separation of the plasma frequencies, the scenario is even qualitatively different [Fig. 3(b)]. Coupling to the second interface is strikingly manifested by the presence of a frequency gap in branch 1, directly recognizable in the ATR spectra of Fig. 2(b) by the disappearance of the second ATR minimum. The cause is that this branch, now at higher energies, is penetrating into the region left of the propagation border $\omega_{\mathrm{PB2}} = \sqrt{(\omega_{\mathrm{p2}}^2 + c^2k^2)/\epsilon_B}$ of the GaZnO♯2 layer (Supplemental Material [16]). While it would stop there for lossless media (for $d < \infty$), the finite damping creates SPPs still left of this borderline. However, the propagation depth into GaZnO♯2 increases and diverges eventually at the branch cuts. Close to the photon line, branches 1 and 2 cross within standard numerical accuracy. There is almost no coupling of the SPPs in the vicinity of this point as their penetration depth into the GaZnO♯1 layer is markedly smaller than the interface separation. Again, one branch approaches a finite frequency for $k \to 0$, characteristic of a metal-metal SPP.

The part of the dispersion still left for experimental verification is accessible by free-space excitation. The real part of the dielectric function of the GaZnO layer No. 1 is negative at the relevant frequencies. Therefore, an evanescent wave is generated at the air/GaZnO♯1 interface, probing the SPPs at the second interface in analogy to the Kretschmann ATR method. Reflection (R) spectra obtained in this mode indeed show a lowered signal in the target range for TM polarization [Fig. 2(c), lower panel]. However, additional measurements of the sample transmission (T) allow for construction of absorption spectra $A = 1 - R - T$ [Fig. 2(c), upper panel] that exhibit well-separated features in TM geometry convincingly confirming excitation of the SPPs in question. For both samples A and B, the experimental points derived from these spectra in conjunction with corresponding TRMA calculations match well to the expected dispersion curves left of the photon line.

In conclusion, the use of a heavily doped semiconductor has allowed for the implementation of a metal-metal SPP dispersion with finite frequency in the long-wavelength

limit. The excitations are robust as $\mathrm{Re}\,\omega \gg |\mathrm{Im}\,\omega|$ always holds. Moreover, coupling of metal-metal and metal-air SPPs in a two-interface configuration has been observed. In the present study, we have restricted ourselves to the role of the doping level in the formation of the coupled-mode dispersion. The interface separation is a further parameter so that practically arbitrary and unique dispersion curves can be shaped. In particular, n-GaZnO can realize these features in a broad range of the infrared spectrum, even up to telecommunication wavelengths. We finally emphasize that the above findings expose a rich potential for the realization of various novel plasmonic schemes, in both fundamental and practical directions. Propagation control by group velocity adjustment is obvious. Furthermore, the dispersion of the metal-metal branch in the vicinity of $k = 0$ is redolent to polaritons in a photonic microcavity. Owing to the bosonic nature of plasmons, macroscopic occupations or even a condensate might, thus, be achievable. Another example is the transfer of nonlinear parametric processes from the optical to the plasmonic domain [17]. The dispersion of sample B already fully satisfies the frequency and phase matching conditions ($\omega_2 = 2\omega_1$, $k_2 = 2k_1$) required for plasmonic second-harmonic generation. Many more examples can be added. Given the advanced possibilities to structure semiconductors down to the nanometer-length scale, we anticipate novel plasmonic functional elements and devices even beyond the planar setting of our study.

This work was supported by the Deutsche Forschungsgemeinschaft in the frame of SFB 951 (HIOS). S. K. thanks the Helmholtz-Energie-Allianz for funding.

[1] R. H. Ritchie, Phys. Rev. **106**, 874 (1957).
[2] W. L. Barnes, A. Dereux, and T. W. Ebbesen, Nature (London) **424**, 824 (2003).
[3] J. A. Schuller, E. S. Barnard, W. Cai, Y. C. Jun, J. S. White, and M. L. Brongersma, Nat. Mater. **9**, 193 (2010).
[4] D. K. Gramotnev and S. I. Bozhevolnyi, Nat. Photonics **4**, 83 (2010).
[5] S. Kawata, Y. Inouye, and P. Verma, Nat. Photonics **3**, 388 (2009).
[6] G. B. Brolo, Nat. Photonics **6**, 709 (2012).
[7] A. Boltasseva and H. A. Atwater, Science **331**, 290 (2011).
[8] G. V. Naik, J. Kim, and A. Boltasseva, Opt. Mater. Express **1**, 1090 (2011).
[9] H. Kim, M. Osofsky, S. M. Prokes, O. J. Glembocki, and A. Piqué, Appl. Phys. Lett. **102**, 171103 (2013).
[10] D. C. Look and K. D. Leedy, Appl. Phys. Lett. **102**, 182107 (2013).
[11] S. Sadofev, S. Kalusniak, P. Schäfer, and F. Henneberger, Appl. Phys. Lett. **102**, 181905 (2013).
[12] P. Halevi, Phys. Rev. B **12**, 4032 (1975).
[13] F. Abeles and T. Lopez-Rios, in *Surface Polaritons, edited by V. M. Agranovich and D. L. Mills (North-Holland, Amsterdam, 1982) and references therein.*
[14] S. L. Cunningham, A. A. Maradudin, and R. F. Wallis, Phys. Rev. B **10**, 3342 (1974).
[15] G. N. Zhizhin and V. A. Yakovlev, in *Surface Polaritons, edited by V. M. Agranovich and D. L. Mills (North-Holland, Amsterdam, 1982) and references therein.*
[16] See Supplemental Material at http://link.aps.org/supplemental/10.1103/PhysRevLett.112.137401 for details about the coupled SPP dispersions and spectra evaluation.
[17] M. Kauranen and A. V. Zayats, Nat. Photonics **6** 737 (2012).